Cold Regions Science and Technology 145 (2018) 127–134

Contents lists available at ScienceDirect

Cold Regions Science and Technology

journal homepage: www.elsevier.com/locate/coldregions

Monitoring mass movements using georeferenced time-lapse photography: Ritigraben rock glacier, western Swiss Alps

Robert Kenner[a,*], Marcia Phillips[a], Philippe Limpach[b], Jan Beutel[c], Martin Hiller[a]

[a] WSL Institute for Snow and Avalanche Research SLF, Davos, Switzerland
[b] ETH Zürich, Institute of Geodesy and Photogrammetry, Switzerland
[c] ETH Zürich, Computer Engineering and Networks Laboratory, Switzerland

ABSTRACT

An automatic method was developed to monitor rock glacier kinematics. Displacements derived from monoscopic time-lapse images were scaled and projected into the Swiss Coordinate System CH1903. We tested this method at the front of the rapidly creeping Ritigraben rock glacier, where time-lapse pictures of the rock glacier front were taken by an automatic camera with a temporal resolution of 3 h. The images were automatically processed using a Matlab algorithm. The output data were spatially resolved creep velocities between successive images and mean relative velocities over time. The digital elevation model used for the projection of the time-lapse data was acquired using terrestrial laser scanning (TLS). The resulting horizontal displacement velocities and accelerations were validated against GPS data measured at one point on the rock glacier front. The high temporal resolution of the time-lapse image velocities provided new insights on the kinematics of the rock glacier front, which could not have been discerned with the GPS or TLS measurements applied. The Ritigraben study site is particularly suitable for our approach due to the temporally constant movement directions. Snow coverage and fog are disturbing factors which can lead to failure of the method.

1. Introduction

Potentially hazardous mass movements such as debris flows and rockfall are a major challenge in populated alpine regions (Pradhan and Buchroithner, 2012). The long-term monitoring of such processes is expensive and complicated, especially in inaccessible mountain terrain. In addition, current climate conditions are contributing towards an increase in the displacement velocities of loose rock material in alpine permafrost environments (Kääb et al., 2007; Delaloye et al., 2010; Kenner et al., 2017), due to phenomena such as warming permafrost substrates and active layer thickening (Zenklusen Mutter et al., 2010; PERMOS, 2013), combined with intensifying rainfall in summer (Scherrer et al., 2016). This development multiplies monitoring tasks and leads to rising costs and logistic challenges, especially in long alpine valleys with numerous lateral sediment providers such as rock glaciers or moraines. Simple low-cost solutions allowing observation of velocities and changes in the kinematics of mass movements are therefore of great interest for the safety managers of exposed transport lines and settlements.

Monoscopic time-lapse photography has long been established as a simple and effective low-tech monitoring method (Bozzini et al., 2012), and is often used to visualize mass wasting processes (Delaloye et al., 2013; van Herwijnen et al., 2013). Time-lapse photography gives a visual impression of the processes occurring and allows an approximation of process kinematics and their extent. In addition, the timing of events such as rock slope failures or debris flows can be established.

Monoplotting, i.e. the projection of photographs onto a digital terrain model (DTM), is often used to georeference image information for further analysis, e.g. for snow line tracking (Schröter and Buchroithner, 2015) or to establish rock glacier extents (Scapozza et al., 2014). This study presents a combination of time-lapse photography and monoplotting, with the aim to quantify displacement velocities of a moving sediment mass and to determine accelerations or changing velocity patterns. Previous studies mainly focused on stereo image pairs to realize this (Kaufmann, 2012; Neyer et al., 2014; Teng et al., 2017), but a few studies already applied a similar approach to monitor glaciers (Maas et al., 2010) or landslides (Travelletti et al., 2012).

We are tracking displacements of an active and potentially hazardous rock glacier front on monoscopic time-lapse images taken by an automatic camera, which are then projected in global coordinates using a monoplotting approach and finally scaled based on a reference measurement with an area-covering 3D measurement system such as

* Corresponding author.
E-mail address: kenner@slf.ch (R. Kenner).

http://dx.doi.org/10.1016/j.coldregions.2017.10.018
Received 3 March 2017; Received in revised form 9 September 2017; Accepted 20 October 2017
Available online 21 October 2017
0165-232X/

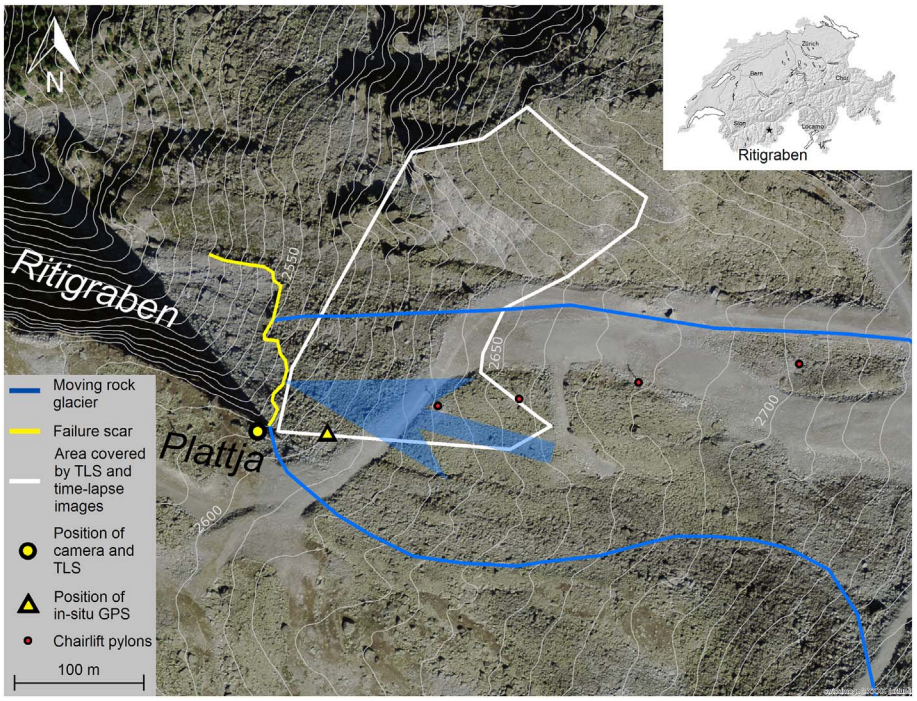

Fig. 1. Orthophoto of the front of the Ritigraben rock glacier with the measurement setup. Equidistance: 10 m, see legend for further details. Inset: map of Switzerland showing the location of Ritigraben. Swissimage© 2016 swisstopo (DV 033594).

terrestrial laser scanning. This procedure was implemented in a fully automatic algorithm and can provide displacement data at a high spatial and temporal resolution. The results are validated against GPS data from a permanent monitoring station on the rock glacier front.

2. Site description

The method presented here was tested on the active, ice-rich Ritigraben rock glacier in the western Swiss Alps above Grächen in Canton Valais (Fig. 1). The rock glacier front is located at around 2600 m a.s.l and flows into the upper end of the WNW oriented 30–40° steep Ritigraben gully at a rate of around 2 m per year. Rockfall periodically occurs here and rock debris accumulates in the gully, where debris flows are regularly released. In the 1990s large debris flows also released directly from the rock glacier tongue in the top of the Ritigraben gully, damaging roads and infrastructure below (Lugon and Stoffel, 2010; Stoffel, 2010). The Plattja rock ridge to the south of the gully is stable and there are two steel pylons (Plattja chairlift) at its eastern end, on the edge of the cliff above the Ritigraben gully. The time-lapse camera described below is attached to one of these pylons (Fig. 1) and the GPS device is located in the topmost southeastern corner of the gully on a large rock moving with the rock glacier (Figs. 1 and 2). The chairlift pylons and cables are visible in the top right part of Fig. 2 and the displaced foundation of a former chairlift pylon which was located on the rock glacier is visible near the centre of the photograph (black arrow), giving a first impression of the kinematics of the rock glacier. In the Ritigraben gully the rock glacier surface is very rough and consists of large boulders with a maximum size of a few cubic metres (Fig. 2). The deformation velocity patterns and their driving factors are analysed in detail by Kenner et al. (2017).

3. Methods

3.1. Terrestrial laser scanning

Terrestrial laser scanning (TLS) has been carried out once annually at the study site since 2012 (Table 1) to monitor the creep behaviour of the Ritigraben rock glacier. The scans were carried out from the Plattja ridge south of the Ritigraben gully (Figs. 1 and 3b) using a Riegl VZ6000 long range laser scanner. The resolution of the resulting point clouds was higher than 10 cm and they were transformed into digital elevation models (DEMs) with a 20 cm resolution. Elevation changes were tracked by calculating difference DEMs. To calculate the horizontal component of the creep movement (position displacements), the

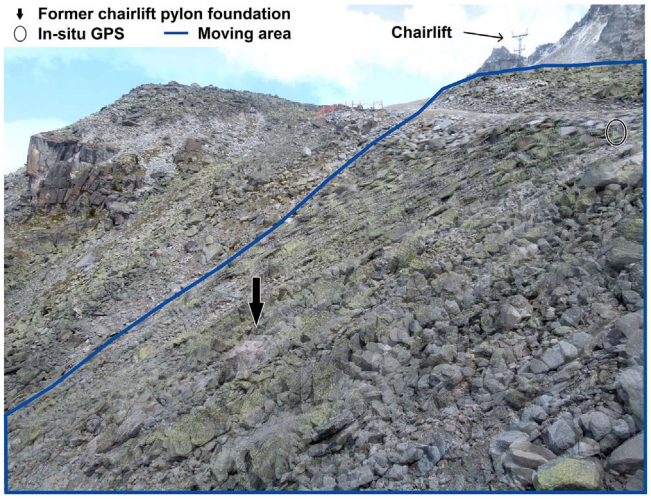

Fig. 2. Two overlying time-lapse images of the Ritigraben rock glacier front taken in July and October 2015. The displacement area is outlined in blue. The former chairlift pylon foundation is shown (black vertical arrow), as are the chairlift and the GPS device. (For interpretation of the references to colour in this figure legend, the reader is referred to the web version of this article.)

Table 1
Measurement dates.

Datasets	Acquisition dates
TLS	12 July 2012; 13 September 2013; 20 August 2014; 11 August 2015
GPS	Since 20 July 2012; 30 s. RAW L1-GPS sampling, 120 s. inclinometer sampling
Time-lapse photography	Since 03 July 2015; every 3 h

Fig. 3. Photographs of the time-lapse camera on the pylon (a), the terrestrial laser scanner next to the pylon (b) and the GPS device (c).

surface structure was extracted from the DEM using a high pass filter and creep rates were then obtained by matching surface structure patterns as described by Kenner et al. (2014). The spatial resolution of these creep rate vector fields was approximately 5 m. Faulty correlations were eliminated by applying a filter kernel to the vector field. This filter algorithm is explained in detail in Section 3.3.2, where it is applied to a vector field obtained from time-lapse photography.

3.2. Continuous differential L1-GPS

The L1-GPS device used here is a custom built GPS data logger with an integrated two-axis inclinometer, ruggedized for long-term outdoor use (Wirz et al., 2014). It is located on a large boulder of the rock glacier on the orographic left part of the rock glacier front (Figs. 1 and 3c). The device uses a commodity u-blox LEA-6T L1-GPS receiver, an active Trimble Bullet III antenna, two Murata SCA830-D07 inclinometers and a Sensirion SHT 21 temperature and humidity sensor IC, powered by a 12 V solar system (30Wp, 33 Ah). All electronics and the antenna are integrated inside the top of a 1 m long fiberglass tube mounted on a steel base. This provides maximum protection, minimizes cabling and elevates the sensitive GPS antenna above the snow cover. The length of the tube increases the radial distance of the GPS antenna from the rotation axis of the block. Tilting of the block can cause significant displacements of the antenna, superimposing the creep signal. These effects can at least partly be corrected by the inclinometer measurements; however the unknown dimensions of the block can cause uncertainties.

The GPS logger is configured for continuous operation with static sampling intervals (Table 1). The logger data is collected annually and fed into a database and post-processing toolchain. For double-differencing differential GPS processing a reference position with an identical GPS receiver setup is used. This reference is located at a stable position with a baseline distance of 5.845 km and an elevation difference of 102 m (WGS84: N 46.12350, E 7.82129).

The GPS data is processed with the Bernese GNSS Software (Dach et al., 2007) in a fully automated processing chain. The processing is based on single frequency differential carrier phase techniques. In this context, daily static coordinates are computed.

To calculate velocities from the GPS position data, the coordinate time series was first filtered using a running mean over 10 days, the period we found to be sufficiently long to remove most of the GPS measurement noise. Within the filtered series, velocities were calculated between the first and the last position values of a 10 day window which was moved along the time series with a daily increment.

3.3. Automatic calculation of global displacement data from time-lapse photography

A MATLAB algorithm was developed, which calculates translation vector fields (TVF) between subsequent images of a time lapse series, automatically corrects offsets between the photographs, deletes translation vectors with faulty correlations, georeferences the TVF, scales the magnitude of the vectors from image to metric units, reorients the vectors within the global coordinate system, resamples the TVF to a regular grid in the global coordinate system and calculates velocities, velocity time series and accelerations.

3.3.1. Feature tracking between subsequent images

A time-lapse camera (Panasonic Lumix DMC FZ100) was installed on a steel chairlift pylon on the stable Plattja ridge above the southern edge of the upper Ritigraben, opposite the detachment zone of the rock glacier (Figs. 1 and 3a). The camera is equipped with a solar panel and takes photographs of the rock glacier front every 3 h (Table 1). The images are registered using an eyefi SD card and transmitted via WLAN from the card to a mobile modem (Netmodule router NB1600). They are then transferred to an online server. The orientation of the camera is fixed and all photographs have approximately the same extent (Fig. 2). Changes in the structure of the rock glacier front can be tracked automatically using the particle imaging velocimetry method introduced by Roesgen and Totaro (1995). This algorithm correlates small patches of the photographs and calculates translation vectors for image patterns that have moved within the images.

These translation vector fields (TVF) are the basis for the automatic monitoring method introduced in this paper. The TVF were calculated with a resolution of 75 pixels and the correlation window size was 150 × 150 pixels. The translation vectors thus form a regular grid on the image. In their initial state, the TVF refer to image coordinates.

3.3.2. Error correction of the translation vector fields

Slight camera movements caused by thermal influences or wind can lead to distortions in the TVF. There can be orientation changes if the camera moves around one of its axes or positioning changes if the whole camera is relocated. Together with orientation changes, also the radial distortion of individual object points can change. As changes in orientation were very small in our case, this error was not measurable in our setup and neglectable. Additionally, orientation changes lead to image wide constant offsets between subsequent photographs. If the camera moves around the y-axis it leads to a rotation of the image. In contrast to orientation changes, positioning changes will cause differential distortions in the TVF which are difficult to correct.

Due to the stability of the mounting point, no position errors occurred. Equally, no rotation was evident and is probably uncommon in general, as this would require a torsion of the mounting structure, which is rather unlikely. The main errors affecting our measurements were occasionally occurring offsets, which became apparent via homogeneous and mono-directional TVF over the entire image extent.

We identified offsets between chronologically successive images by defining a reference patch within the images, located in stable rock areas. If translation vectors appear in these areas, they define the vertical and horizontal components of an offset. The whole TVF was therefore corrected using these values.

Another error occurs in parts of the image where patterns change rapidly (e.g. sky, fast rock slides and rockfall). Here the TVF is chaotic and contains mismatches. Faulty correlations were eliminated by applying a 3 × 3 deleting kernel to the gridded TVF. If the standard deviation of the vector directions within the kernel exceeded 10°

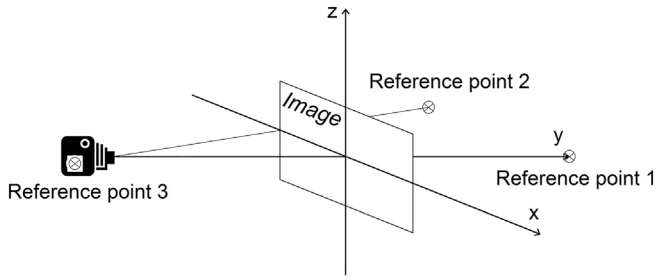

Fig. 4. Sketch showing the definition of the camera coordinate system using reflecting control points.

(empirically defined value), the central vector was deleted. To restore erroneously deleted values surrounding zones with faulty correlations, a 3 × 3 dilation was subsequently applied (Kenner et al., 2014).

3.3.3. Georeferencing of the translation vector fields

The georeferencing of the translation vectors was realized by creating a transformation mask based on the 2015 TLS point cloud. The high resolution point cloud (< 10 cm) of the rock glacier front was captured from a position 2 m south of the camera with a similar perspective as that in the time-lapse photographs. To reference the laser scan point cloud on the photographs, reflecting reference points were temporarily installed on the rock glacier: one at the point representing the image centre, one on the left end of the line bisecting the image horizontally and another on the camera box. Using these three points, a Cartesian camera coordinate system was defined with the y-axis originating in the focal point of the camera and going through the image centre, the x-axis running orthogonal to the y-axis and lying in the plane defined by the three reference points and the z-axis perpendicular to x and y (Fig. 4). After the point cloud was transformed into Cartesian camera coordinates, a second transformation into image coordinates was applied by calculating a central projection of the point cloud from the position of the camera using:

$$x_i = c \bullet \frac{x_c}{z_c} \bullet s + a$$

$$y_i = c \bullet \frac{y_c}{z_c} \bullet s + a$$

where x_i; y_i are image coordinates, x_c; y_c; z_c are camera coordinates, c is the focal length of the camera, s is the scale factor and a the additional constant between both coordinate systems. After the point cloud was projected onto the images, it was transformed into a 3-band raster dataset with 1/10 of the photo resolution, containing information on the global x, y and z coordinates of the original laser scanning points. If one raster cell contained > 1 TLS point the coordinate information was averaged, which led to a smoother representation of the surface. Each translation vector was then georeferenced by assigning the global coordinate information from the underlying raster cell to it.

3.3.4. Orientation and scaling of the translation vector fields

Although the TVF were georeferenced now, they still contained displacement values in image units (pixels) and a displacement direction was missing. Thus, further masks for the scaling and orientation of the translation vectors were created. To do this, we compared image-based TVF $A = \left(\overrightarrow{a_{ij}}\right)$ (in image units) and TLS creep vectors $B = (\overrightarrow{b_{ij}})$ (in global units). As the measurement periods of both methods differ, B (annual basis) was normalized on A (5 month basis) using the continuous GPS time series:

$$B_{timelapse,period} = \frac{B_{annual} \bullet \Delta GPS_{timelapse,period}}{\Delta GPS_{annual}}$$

Each $\overrightarrow{a_{ij}}$ was then linked to a distance weighted mean value $\overrightarrow{\overrightarrow{b}}$ of

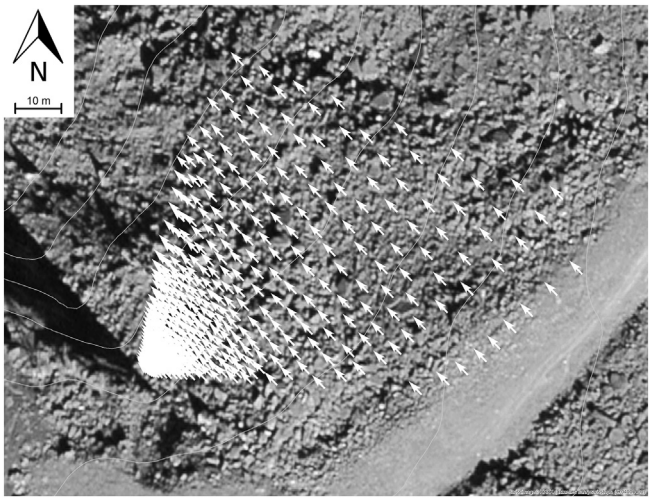

Fig. 5. Raw translation vector field prior to resampling and scaling, showing the influence of the central projection on its spatial resolution. Swissimage© 2016 swisstopo (DV 033594).

the $\overrightarrow{b_{ij}}$ surrounding it. The scaling factor for $\overrightarrow{a_{ij}}$, s_{ij}, was simply obtained by $s_{ij} = \frac{|\overrightarrow{\overrightarrow{b}}|}{|\overrightarrow{a_{ij}}|}$. The azimuth az_{ij} for $\overrightarrow{a_{ij}}$ was adopted from $\overrightarrow{\overrightarrow{b}}$. As a result, we obtained the scaling mask $S = (s_{ij})$ and the azimuth mask $AZ = (az_{ij})$ which allow to attribute each image-based translation vector of any TVF with an individual universally valid scaling factor and azimuth.

The image-based TVF now contained horizontal 2D displacements of the rock glacier surface in metric units; however their spatial resolution was still affected by the central projection of the camera (Fig. 5). Therefore the TVF was resampled in a regular grid with a defined spatial resolution of 2.5 m. Vectors in parts of the TVF with originally higher resolutions were merged by weighted averaging.

3.3.5. Calculation of velocity time series

As the algorithm processes any number of chronologically successive images, it not only calculates surface displacements but also velocities, velocity time series and accelerations. The time-lapse between the images is used to calculate mean daily creep velocities for every translation vector. These spatially variable creep velocities are summarized to a mean relative velocity, on the basis of a reference velocity defined by the first two images within the series. Each velocity vector between images i and i + 1 is expressed as a fraction of the velocity vector at the same location between images 1 and 2, expressed as a percentage. The spatial mean of these values can be based on a strongly varying number of single vectors, depending on how many have passed the filter algorithm; the number of vectors the mean velocity is based on is therefore outputted, specifying the statistical basement of the mean velocity. The time series of the relative velocity are shown in chart form and the absolute velocities are produced as vector fields in shapefile format. Similar outputs are also available for acceleration values.

3.4. Accuracy analyses

3.4.1. Sensitivity of the approach to different error sources

The method presented here produces two kinds of output, spatially and temporally resolved absolute displacement data and a relative velocity time series. The relative velocity time series is only affected by errors originating from the image quality. This refers to factors such as the stability of the camera frame, the geometry of the photograph (distance and angle to the moving object), the image resolution and the light and contrast conditions in the photograph. The actual accuracy reached here becomes evident in the reproduction of unchanged terrain

parts or in the reproducibility of the velocity time series.

The absolute displacement values are affected by more error sources. As they are based on the TLS measurements (basis for the scaling mask), the TLS accuracy is a limiting factor. Additionally, georeferencing errors and the spatial resolution of the scaling mask play a role. Georeferencing is important to attribute the correct scaling factor from the scaling mask to each translation vector. A high spatial resolution of the scaling mask reduces the error introduced when interpolating the scaling factors surrounding a translation vector. Visual checks of the georeferencing results were carried out by overlaying the images with the projected point cloud used to define the georeferencing mask. A comparison of characteristic objects in the point cloud and the image revealed that the georeferencing error is within the range of a few pixels. This corresponds to < 10 cm georeferencing error within the movement zone. Considering that the spatial resolution of the scaling mask is 4.75 m, such a small georeferencing error is not very relevant. Also a higher resolution of the scaling mask would have limited benefits: the rock glacier movement is spatially quite homogeneous and except from the boundary zones of the movement there is little change in velocity within a radius of 4.75 m.

3.4.2. Accuracy of TLS and GPS measurements

A comprehensive accuracy analysis for TLS measurements on alpine mass movements was carried out by Kenner et al. (2014) for comparable study sites with creeping permafrost features. This study gives a reliable rule of thumb for the accuracy estimation of TLS derived creep vector fields: offsets between the underlying DEMs become evident in homogeneous vector fields outside the moving areas. Provided that there are no such offsets, the smallest deformation vectors remaining after the application of the filter algorithm give a good approximation of the accuracy obtained for the deformation values. Kenner et al. (2014) specified that the accuracy commonly reached for TLS derived translation vectors on rock glaciers is around 2–3 cm. In the case of Ritigraben, there is no offset between the scanned DEMs and the smallest remaining vectors are 3 cm.

The daily GPS coordinates are estimated with an error (standard deviation) of approximately 1–2 mm in the horizontal and 2–3 mm in the vertical component. Hence, the accuracy of the GPS method is around one order of magnitude higher than that of TLS and it provides a much higher temporal resolution, however only at a point scale.

3.4.3. Accuracy of the displacement data obtained from time-lapse image processing

The accuracy of the relative creep velocity data obtained with time-lapse photography was analysed by comparing relative velocity time series of two image time series within the same monitoring period (3 July to 19 November 2015). Both time series consisted of images with an approximately weekly resolution but the acquisition time of the individual photographs differed by a few hours, yet by < 24 h (Table 2). Only the first two images of both data series were identical, as they define the reference velocity (100%) for the subsequent relative velocity values. Data from both time series was treated as being comparable, although the acquisition time differed slightly. The root mean square error (RMSE) between both velocity time series was calculated to quantify the internal robustness of the method, i.e. the reproducibility of the results. Using this procedure the effects of different lighting conditions or small movements of the camera (e.g. induced by vibrations of the pylon) within the time series could be analysed.

We also compared the image-based velocity time series with the GPS-based one. The relative velocities from time-lapse images were transformed into absolute velocities by fixing the initial relative velocity (100%) between the first two images to the absolute velocity value obtained by the GPS measurements during the same period. All subsequent relative velocities in the time series were transformed by referring to this initial absolute velocity. Apart from the initial value, the further progression of the image-based absolute velocity time series is therefore independent from the GPS time series.

Table 2
Acquisition dates of the individual images of two parallel time-lapse image series.

Image time series 1	Image time series 2
3 July 2015 14:00	3 July 2015 14:00
10 July 2015 14:00	10 July 2015 14:00
17 July 2015 14:00	17 July 2015 20:00
24 July 2015 14:00	24 July 2015 17:00
31 July 2015 14:00	31 July 2015 20:00
7 August 2015 14:00	7 August 2015 20:00
13 August 2015 14:00	13 August 2015 17:00
21 August 2015 14:00	21 August 2015 20:00
27 August 2015 14:00	27 August 2015 20:00
3 September 2015 14:00	2 September 2015 17:00
10 September 2015 14:00	10 September 2015 08:00
16 September 2015 17:00	16 September 2015 14:00
24 September 2015 14:00	24 September 2015 08:00
1 October 2015 11:00	1 October 2015 08:00
9 October 2015 14:00	9 October 2015 17:00
13 October 2015 08:00	12 October 2015 17:00
22 October 2015 17:00	22 October 2015 08:00
30 October 2015 17:00	30 October 2015 08:00
5 November 2015 17:00	5 November 2015 08:00
12 November 2015 17:00	12 November 2015 08:00
19 November 2015 08:00	20 November 2015 08:00

4. Results and discussion

The TLS measurements show an unchanged geometry of the rock glacier body with constant movement directions during the period 2012 to 2015. A detailed analysis of the rock glacier deformation velocity can be found in (Kenner et al., 2017).

Two synchronous time series of the relative velocity based on different images with varying lighting conditions (different shadow patterns, cloud cover) showed a high degree of consistency (Fig. 6). The RMSE between them is 5.6% relative velocity, referring to an initial absolute velocity (mean velocity between the first two images) of 4.0 mm/day. This good reproducibility implies a high level of robustness despite different lighting conditions or small changes in the camera orientation. Travelletti et al. (2012), who monitored a landslide with a similar method reported larger influences by these factors. This might be caused by longer measurement ranges and a less clearly defined surface structure. However, also our offset correction and the different way of filtering the vector fields probably reduced these error influences here.

When compared to the GPS measurements, the velocities based on time-lapse images are reasonable and show similar magnitudes. Fig. 7 displays the spatial mean of the relative velocity of the rock glacier front for the complete time-lapse data series acquired in summer 2015, supplemented by GPS velocities. Both velocity charts show a similar overall progression but velocity variations at time scales of days to one week are not reflected in the GPS time series (Fig. 7). This is caused by methodical differences: The time-lapse method has a fixed level of significance for which surface displacements can be tracked. This level of significance is independent from the length of the time-lapse between the images. Hence, short term accelerations can be tracked at any temporal resolution if the velocity is high enough. In contrast, L1 GPS measurements rely on redundancy to reach their full potential in accuracy. This implies a limitation for the temporal resolution of significant GPS velocities, as measurements over a certain time period have to be integrated to obtain the required redundancy. Generally it is difficult to differentiate between short term accelerations and GPS measurement errors (Wirz et al., 2014) and the definition of the optimal temporal resolution for GPS based velocity time series is therefore challenging. Our GPS velocities are derived with a temporal resolution of 10 days and are additionally smoothed by a running mean. Velocity

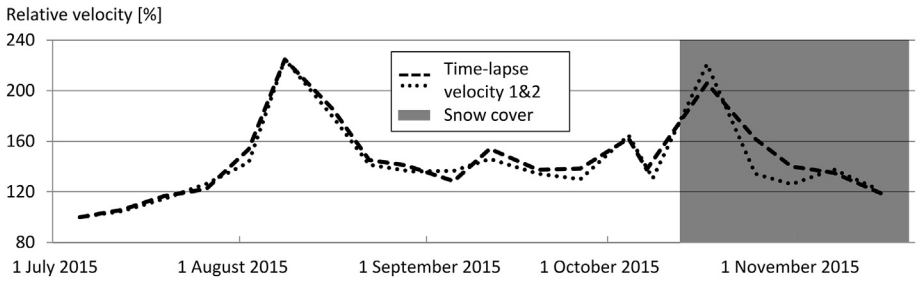

Fig. 6. Rock glacier velocities derived from 2 differential time-lapse image series.

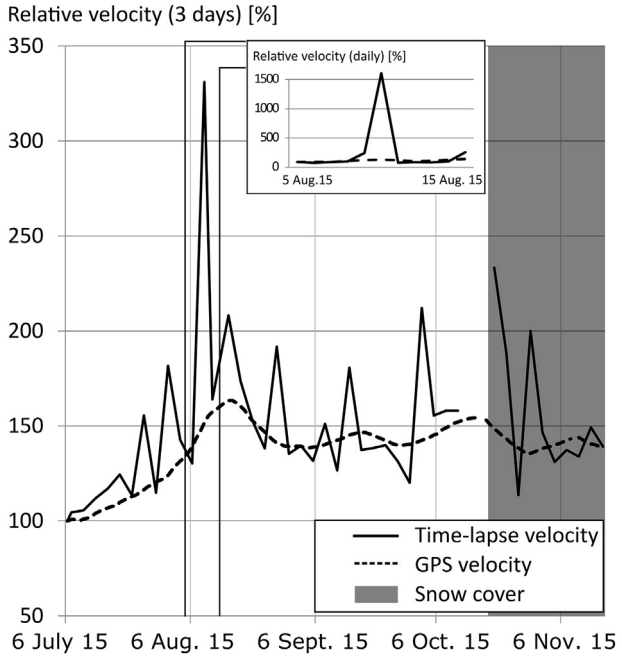

Fig. 7. Comparison of rock glacier velocities derived from GPS and time-lapse photography with a 3 day temporal resolution. The inset contains a close up of the period 5 to 15 August 2015 with daily resolution, showing a strong acceleration between 9 and 10 August.

maxima of short term accelerations are therefore smaller or absent in the GPS time series compared to the time-lapse image based velocities. These systematic differences became evident in particular between 9 and 10 August 2015. In this short period the rock glacier front accelerated 16-fold, as is clearly shown by the time-lapse velocity chart (Fig. 7, inset) and is visible to the naked eye in the images. This velocity peak is however strongly smoothed in the GPS velocity data.

An additional difference between the GPS and image based velocities becomes evident in the mean seasonal displacement values. The seasonal acceleration of the rock glacier (Kenner et al., 2017), which can be particularly well distinguished in July and at the beginning of August (Fig. 7), is less pronounced in the GPS velocity values than in the image based ones. This might be caused by the spatial resolution of the datasets. While the image based velocity time series is calculated over the whole rock glacier front, the GPS time series is based on a point measurement. The GPS sensor is located in a relatively slow sector of the rock glacier front, which probably shows more homogeneous velocities than most of the other parts captured by the time-lapse camera.

Generally, moderate deviations between both systems show that the time-lapse algorithm produced reasonable velocities, even during a period with a slowly melting, thin snow cover of around 20 cm in autumn 2015 (Fig. 7). However, problems occurred when calculating velocities between images with large differences in snow cover, e.g. the differences before and after a snowfall (time-lapse data gap in Fig. 7). Equally, a thick snow cover covering most of the boulders in the moving zone leads to failure of the time-lapse image method. Surface tracking of images from subsequent summer periods were not possible, as the surface structure moved to strong during the winter. However, images acquired with a time lag of several weeks could be processed. This might not be possible for sites with stronger surface changes (Travelletti et al., 2012).

Fig. 8 shows the absolute velocities at the rock glacier front for 8 periods of around 7 days between 10 July and 02 September 2015. The spatially varying velocity patterns over the rock glacier front become evident. For example, in Fig. 8a, the fastest movements occur directly at the failure scar, whilst in Fig. 8h, the fastest zone is in the upper part of the rock glacier front. Such high-frequency measurements are not feasible using manual measurement campaigns. The different extents of the TVF in Fig. 8 have methodical reasons. In the upper part of the rock glacier front the angle of projection of the terrain in the images is glancing, so creep velocities can only be determined during periods with high overall displacements here (e.g. Fig. 8e). Due to the varying extent of the TVF, it is important to calculate the relative velocity on the basis of single vectors and not on the basis of an overall mean velocity.

A further benefit of the time-lapse image monitoring method is that the images are accessible online and the processing can be carried out in near real time. The method therefore has the potential to be applied for early-warning purposes. In addition to displacement data, the images provide visual information on the movement process, on rapid mass movements like rockfall or slides and on environmental conditions such as weather or snow coverage.

The main limitations of the time-lapse method are induced by the requirement that the creep directions and the geometry of the mass wasting area remain approximately constant, as fixed azimuths and georeferencing masks are used. This is certainly the case on the rapidly creeping rock glacier front in the steep and narrow Ritigraben gully. However it is not necessarily the case for other mass movements.

5. Conclusions

Time-lapse photography has proved to be a reliable monitoring system for an alpine mass movement with temporally uniform movement directions and limited changes in overall geometry. Once calibrated by a 3D measurement such as TLS, time-lapse photography provides highly resolved temporal and spatial information on the absolute and relative velocities of the mass movement. This information is useful to determine local or overall accelerations of the moving mass, which often point towards the preparatory phase of a rockfall or debris flow event. For individual cases, time-lapse photography monitoring can therefore be suitable to substitute other, more expensive long-term monitoring systems. We conclude that:

- Displacement vectors derived from time-lapse images can be successfully georeferenced, scaled and oriented using displacement data from a reference period acquired with a 3D measurement system such as terrestrial laser scanning.
- After calibration, time-lapse image monitoring functions independently.
- The complete processing of the time-lapse images can be automated

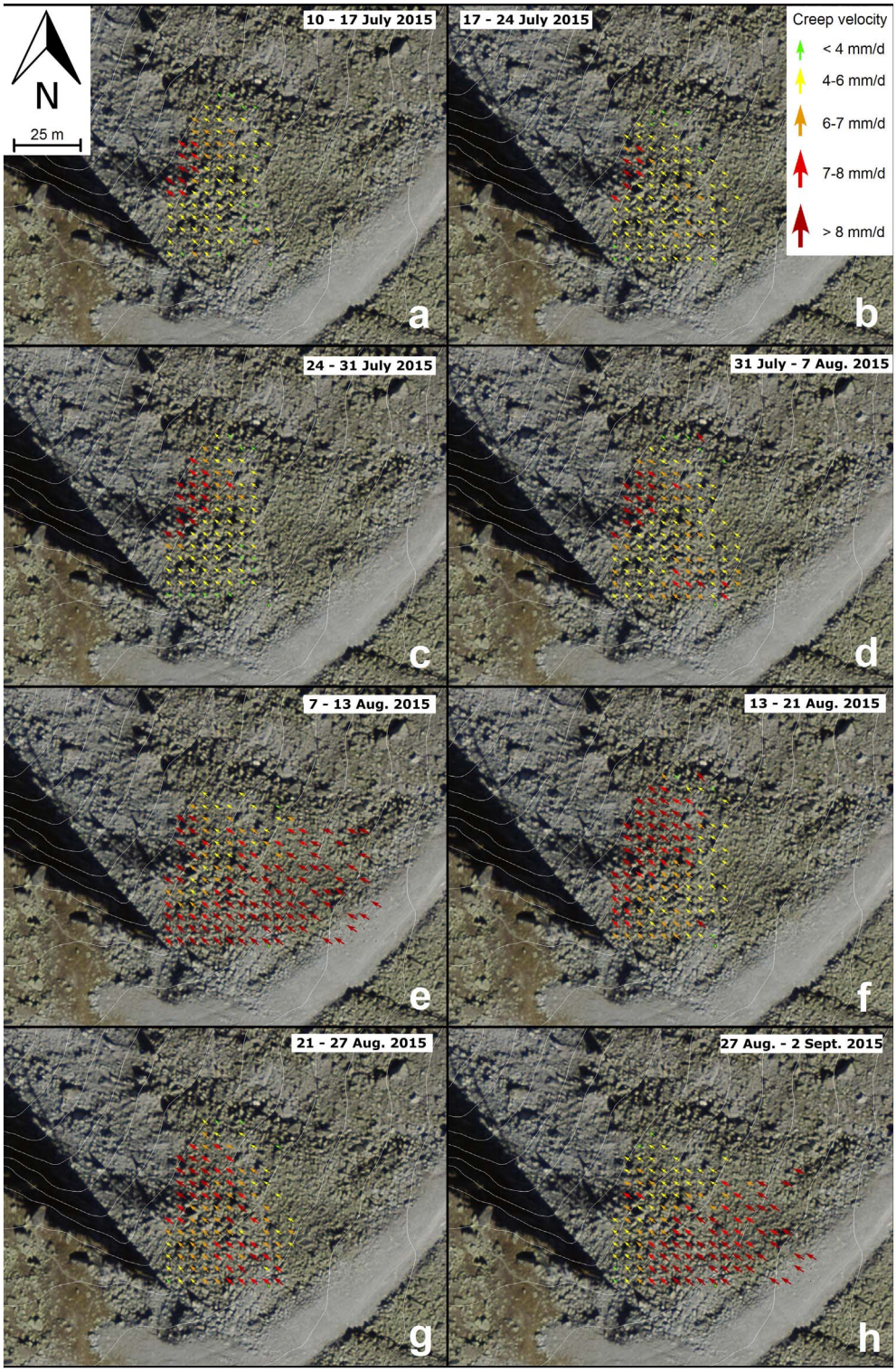

Fig. 8. Spatial velocity distribution for selected 7 day periods in summer 2015 (10 July to 9 September 2015). Swissimage© 2016 swisstopo (DV 033594).

in near real time, with vector shapefiles and velocity time charts as output data.

- Time-lapse image monitoring provides significant velocity data at a very high temporal resolution and captures short term accelerations that are not registered to this extent by permanent GPS measurements.
- Ideally, the camera orientation should be orthogonal to the moving surface to avoid shadow effects and glancing intersections.
- At the Ritigraben site, different lighting conditions do not substantially influence the results of the time-lapse monitoring.
- Strong changes in snow coverage lead to failure of the method, whilst a thin and constant snow cover has little influence.
- The visual impression of the images complements the automatic displacement values with information on fast movements not captured by the algorithm and also allows observation of weather/snow conditions.

Acknowledgements

This project was jointly funded by the Swiss National Science Foundation (SNF) Sinergia project 'TEMPS' (The Evolution of Mountain Permafrost in Switzerland, project no. 136279) and by the Swiss Federal Office for the Environment. The authors sincerely thank Reto Imesch (Bergbahnen Grächen), Martin Volken and Sebastian Summermatter (Geomatik AG, Zermatt), Eric Pointner (Rovina & Partner AG, Varen) and Andreas Hasler (Sensalpin GmbH, Davos) for their valuable technical and logistic support. The terrestrial laser scanner was jointly funded by the SNF and WSL (R'Equip project no. 206021_157774). We are grateful to Canton Valais and the local authorities in Grächen and St. Niklaus for their ongoing interest and support.

References

Bozzini, C., Conedera, M., Krebs, P., 2012. A new Monoplotting tool to extract georeferenced vector data and orthorectified raster data from oblique non-metric photographs. Int. J. Herit. Digit. Era 1 (3), 499–518. http://dx.doi.org/10.1260/2047-4970.1.3.499.

Dach, R., Hugentobler, U., Fridez, P., Meindl, M., 2007. Bernese GPS Software Version 5.0. 640. Astronomical Institute, University of Bern, pp. 114.

Delaloye, R., Lambiel, C., Gärtner-Roer, I., 2010. Overview of rock glacier kinematics research in the Swiss Alps: seasonal rhythm, interannual variations and trends over several decades. Geogr. Helv. 65, 135–145.

Delaloye, R., Morard, S., Barboux, C., Abbet, D., Gruber, V., Riedo, M., Gachet, S., 2013. In: Graf, C. (Ed.), Rapidly Moving Rock Glaciers in Mattertal, Mattertal - ein Tal in Bewegung, St. Niklaus. Eidg. Forschungsanstalt WSL, pp. 21–31.

van Herwijnen, A., Berthod, N., Simenhois, R., Mitterer, C., 2013. Using time-lapse photography in avalanche research. In: Proceedings ISSW, pp. 950–954.

Kääb, A., Frauenfelder, R., Roer, I., 2007. On the response of rockglacier creep to surface temperature increase. Glob. Planet. Chang. 56, 172–187. http://dx.doi.org/10.1016/j.gloplacha.2006.07.005.

Kaufmann, V., 2012. The evolution of rock glacier monitoring using terrestrial photogrammetry: the example of Äußeres Hochebenkar rock glacier (Austria). Aust. J. Earth Sci. 105 (2).

Kenner, R., Bühler, Y., Delaloye, R., Ginzler, C., Phillips, M., 2014. Monitoring of high alpine mass movements combining laser scanning with digital airborne photogrammetry. Geomorphology 206 (0), 492–504. http://dx.doi.org/10.1016/j.geomorph.2013.10.020.

Kenner, R., Phillips, M., Beutel, J., Hiller, M., Limpach, P., Pointner, E., Volken, M., 2017. Factors Controlling Velocity Variations at Short-Term, Seasonal and Multiyear Time Scales, Ritigraben Rock Glacier, Western Swiss Alps. Permafr. Periglac. Process. 28 (4), 675–684. http://dx.doi.org/10.1002/ppp.1953.

Lugon, R., Stoffel, M., 2010. Rock-glacier dynamics and magnitude-frequency relations of debris flows in a high-elevation watershed: Ritigraben, Swiss Alps. Glob. Planet. Chang. 73, 202–210. http://dx.doi.org/10.1016/j.gloplacha.2010.004.

Maas, H.G., Casassa, G., Schneider, D., Schwalbe, E., Wendt, A., 2010. Photogrammetric determination of spatio-temporal velocity fields at Glaciar San Rafael in the Northern Patagonian Icefield. Cryosphere Discuss. 2010, 2415–2432. http://dx.doi.org/10.5194/tcd-4-2415-2010.

Neyer, F., Limpach, P., Gsell, T., Geiger, G., Beutel, J., 2014. Permanent rock glacier monitoring with a stereo pair of optical cameras. In: Oesterling, N., Wiget, A., Cannata, M. (Eds.), Swiss Geoscience Meeting, Fribourg, Switzerland. 381.

PERMOS, 2013. Permafrost in Switzerland 2008/2009 and 2009/2010. In: Noetzli, J. (Ed.), Glaciological Report. University of Zurich, Permafrost.

Pradhan, B., Buchroithner, M., 2012. Terrigenous Mass Movements. Springer-Verlag, Berlin Heidelberg, pp. 400.

Roesgen, T., Totaro, R., 1995. Two-dimensional on-line particle imaging velocimetry. Exp. Fluids 19, 188–193.

Scapozza, C., Lambiel, C., Bozzini, C., Mari, S., Conedera, M., 2014. Assessing the rock glacier kinematics on three different timescales: a case study from the southern Swiss Alps. Earth Surf. Process. Landf. 39 (15), 2056–2069. http://dx.doi.org/10.1002/esp.3599.

Scherrer, S.C., Fischer, E.M., Posselt, R., Liniger, M.A., Croci-Maspoli, M., Knutti, R., 2016. Emerging trends in heavy precipitation and hot temperature extremes in Switzerland. J. Geophys. Res.-Atmos. 121 (6), 2626–2637. http://dx.doi.org/10.1002/2015JD024634.

Schröter, B., Buchroithner, M., 2015. Time-lapse camera images for observation and visualisation of snow lines on glaciers in high Asia. In: International Cartographic Conference, Rio de Janeiro/Brazil.

Stoffel, M., 2010. Magnitude-frequency relationships of debris flows - a case study based on field surveys and tree-ring records. Geomorphology 116, 67–76.

Teng, Y., Stanier, S.A., Gourvenec, S.M., 2017. Synchronised multi-scale image analysis of soil deformations. Int. J. Phys. Modell. Geotech. 17 (1), 53–71. http://dx.doi.org/10.1680/jphmg.15.00058.

Travelletti, J., Delacourt, C., Allemand, P., Malet, J.-P., Schmittbuhl, J., Toussaint, R., Bastard, M., 2012. Correlation of multi-temporal ground-based optical images for landslide monitoring: application, potential and limitations. ISPRS J. Photogramm. Remote Sens. 70, 39–55. http://dx.doi.org/10.1016/j.isprsjprs.2012.03.007.

Wirz, V., Beutel, J., Gruber, S., Gubler, S., Purves, R.S., 2014. Estimating velocity from noisy GPS data for investigating the temporal variability of slope movements. Nat. Hazards Earth Syst. Sci. 14 (9), 2503–2520. http://dx.doi.org/10.5194/nhess-14-2503-2014.

Zenklusen Mutter, E., Blanchet, J., Phillips, M., 2010. Analysis of ground temperature trends in alpine permafrost using generalized least squares. J. Geophys. Res. 115, F004009. http://dx.doi.org/10.1029/2009JF001648.